Supplemental Material for

Theoretical prediction of superconductivity in boron kagome monolayer: MB_3 (M = Be, Ca, Sr) and the hydrogenated CaB_3

Liu Yang (杨柳)[1] , Ya-Ping Li (李牙平)[1] , Hao-Dong Liu (刘浩东)[1] , Na Jiao (焦娜)[1] , Mei-Yan Ni (倪美燕)[1], Hong-Yan Lu (路洪艳)[1,*] , Ping Zhang (张平)[1,2,*], and C. S. Ting[3]

[1]*School of Physics and Physical Engineering, Qufu Normal University, Qufu 273165, China*
[2]*Institute of Applied Physics and Computational Mathematics, Beijing 100088, China*
[3] *Texas Center for Superconductivity and Department of Physics, University of Houston, Houston, Texas 77204, USA*

Corresponding Authors:
*E-mail: hylu@qfnu.edu.cn (H.Y. Lu)
*E-mail: zhang_ping@iapcm.ac.cn (P. Zhang)

Content

1. Computational details

We perform the first-principles calculations within the density functional theory (DFT) to calculate the electronic structure using the Vienna ab-initio simulation package (VASP)[1] and the well-established Quantum-ESPRESSO package[2]. The Perdew-Burke-Ernzerhof generalized gradient approximation (PBE-GGA) is chosen for the exchange-correlation functional[3]. The Projector-Augmented-Wave (PAW) method is adopted to describe the electron-ion interactions. Density functional perturbation theory (DFPT)[4] is used to calculate the dynamics matrix and EPC within the range of linear response and as input to solve the isotropic Eliashberg equation. The cutoffs for wave functions and charge density are set as 80 Ry and 800 Ry, respectively. The convergence criteria for energy and force are set as 10^{-8} eV and -0.03 eV. The vacuum separation is set to 20 Å to avoid coupling between two neighboring monolayers. The ab-initio molecular dynamics (AIMD) simulations in the NVT ensemble are employed to investigate the thermal stability of these 2D MB$_3$ (M = Be, Ca, Sr) monolayers. They are performed by using 5×5×1 supercells with a time step of 1 fs and total simulation of 6 ps. For the calculation of DOS, k-points of 45×45×1 is used. The accurate electron-phonon interaction matrix is calculated on a dense 60×60×1 k-point grid, and a 15×15×1 q-point grid is set to calculate the phonon properties and electron-phonon coupling.

The total electron-phonon coupling (EPC) constant λ is obtained via isotropic Eliashberg function[5-7]:

$$\alpha^2F(\omega) = \frac{1}{2\pi N(E_F)}\sum_{\boldsymbol{q}\nu}\delta(\omega-\omega_{\boldsymbol{q}\nu})\frac{\gamma_{\boldsymbol{q}\nu}}{\hbar\omega_{\boldsymbol{q}\nu}} \quad (1)$$

$$\lambda = 2\int_0^\infty \frac{\alpha^2F(\omega)}{\omega}d\omega = \sum_{\boldsymbol{q}\nu}\lambda_{\boldsymbol{q}\nu} \quad (2)$$

where $\alpha^2F(\omega)$ is Eliashberg function and $N(E_F)$ is the DOS at the Fermi level, $\omega_{\boldsymbol{q}\nu}$ is the phonon frequency of the νphonon mode with wave vector $\boldsymbol{q}$, and $\gamma_{\boldsymbol{q}\nu}$ is the phonon linewidth[5-7]. The $\gamma_{\boldsymbol{q}\nu}$ can be estimated by

$$\gamma_{\boldsymbol{q}\nu} = \frac{2\pi\omega_{\boldsymbol{q}\nu}}{\Omega_{BZ}}\sum_{\boldsymbol{k},n,m}\left|g^{\nu}_{\boldsymbol{k}n,\,\boldsymbol{k}+\boldsymbol{q}m}\right|^2\delta(\varepsilon_{\boldsymbol{k}n}-E_F)\delta(\varepsilon_{\boldsymbol{k}+\boldsymbol{q}m}-E_F) \quad (3)$$

where Ω_{BZ} is the volume of the BZ, $\varepsilon_{\boldsymbol{k}n}$ and $\varepsilon_{\boldsymbol{k}+\boldsymbol{q}m}$ indicate the Kohn-Sham energy, and $g^{\nu}_{\boldsymbol{k}n,\,\boldsymbol{k}+\boldsymbol{q}m}$ represents the screened electron-phonon matrix element. $\lambda_{\boldsymbol{q}\nu}$ is the EPC constant for phonon mode $\boldsymbol{q}\nu$, which is defined as

$$\lambda_{\boldsymbol{q}\nu} = \frac{\gamma_{\boldsymbol{q}\nu}}{\pi\hbar N(E_F)\omega^2_{\boldsymbol{q}\nu}} \quad (4)$$

T_c is estimated by McMillan-Allen-Dynes formula[7]:

$$T_c = \frac{\omega_{log}}{1.2}exp\left[\frac{-1.04(1+\lambda)}{\lambda-\mu^*(1+0.62\lambda)}\right] \quad (5)$$

The hysteretic Coulomb pseudopotential μ^* in Eq. (5) is set to 0.1 and logarithmic average of the phonon frequencies ωlog is defined as

$$\omega_{log}=exp\left[\frac{2}{\lambda}\int_0^\omega \alpha^2F(\omega)\frac{ln\omega}{\omega}d\omega\right] \quad (6)$$

For the calculation of superconducting properties, the δ functions for electrons and phonons are smeared out by a Gaussian function with the broadening of 0.01 Ry and 0.16 THz, respectively.

2. Lattice structure and stability of BeB_3 and SrB_3

The lattice structure of BeB_3 and SrB_3 are shown in Fig. S1 (a,b). After fully optimization, the structure parameters of BeB_3 and SrB_3 are 3.464 Å and 3.465 Å, respectively. The heights of Be and Sr to boron kagome lattice (*h*) are 0.65Å and 2.30 Å, and the B-B bond lengths are the same, i.e., 1.732 Å. The AIMD shows the variation of free energy of BeB_3 and SrB_3 within 6 ps, along with the last frame of the photographs in Fig. S1(c) and Fig. S1(d) for BeB_3 and SrB_3, respectively. The structure stability is maintained at 400 K for BeB_3 with the energy fluctuates around -556.5 eV and at 220 K for SrB_3 with the energy fluctuates around -488.5 eV. In Fig. S1(e，f), the charge density difference clearly shows the charge transfer for BeB_3 and SrB_3.

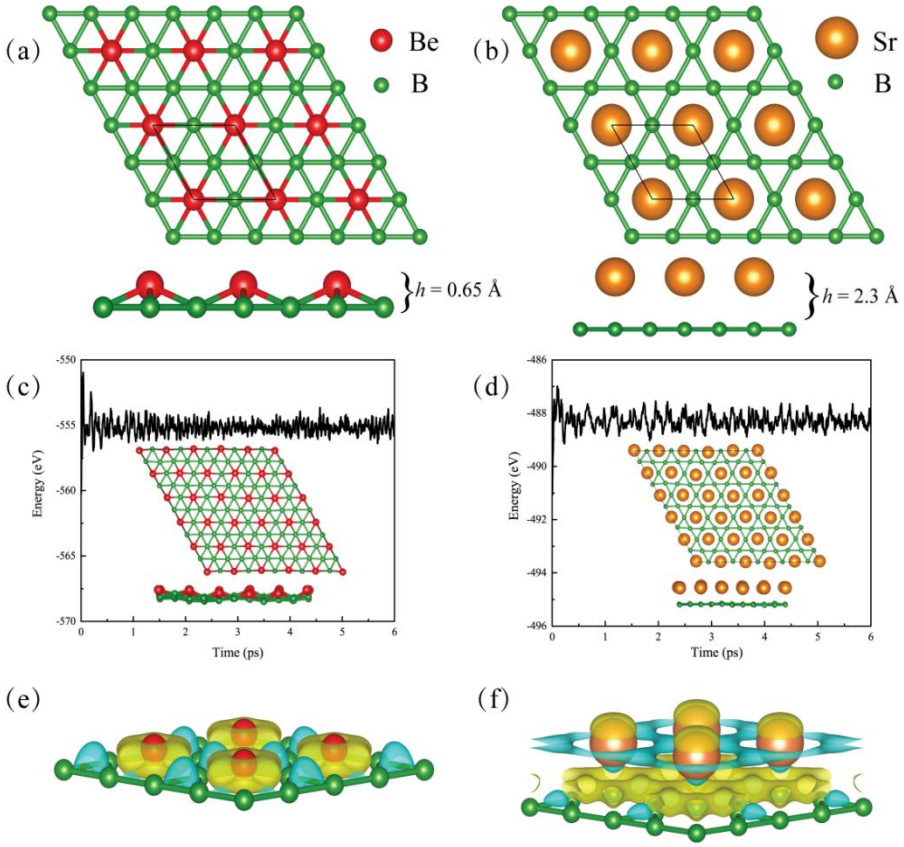

Fig. S1: Top and side views of the lattice structures of BeB_3 (a) and SrB_3 (b). Green (red, orange) spheres represent B (Ca, Sr) atoms and the unit cell is shown. *h* is the perpendicular distance between metal atoms and B kagome lattice. (c) and (d) The variation of the free energy in the AIMD simulations during the time scale of 6 ps along with the last frame of photographs at 400 K for BeB_3 and 220 K for SrB_3, respectively. (e) and (f) Charge density difference for BeB_3 and SrB_3. The color blue (yellow) represents the area where electrons are lost (obtained).

3. Final relaxed positions of H atoms in $HCaB_3$

We have considered several possible structures of hydrogenated monolayer CaB_3. Within the CaB_3 unit cell, there are four highly symmetric positions where the H atoms can occupy. The initial positions of H atoms above the center of triangle formed by B atoms, above the B and Ca atoms, and above the B-B bonds are shown in Figs. S2(a-d). After full relaxation, the corresponding final positions of H atoms are shown in Figs. S2(e-h). For the H atoms above the B and Ca atoms, only the height of them changes after full relaxation, as seen in Fig. S2(f) and S2(g). From Figs. S2(d)

and 2(h), it is clearly seen that H atoms move from above the B-B bonds to the hollow center of the B triangles, which is the same with that in Fig. S2(e). The calculated final total energies for the structures in Figs. S2(e-h) are -24.9, -24.6, -22.8, -24.9 eV/cell, respectively. Thus, the configuration with H atoms above the center of triangle formed by B atoms in Fig. S2(e) shows the lowest energy, and it is the most stable structure. We choose this configuration to study the superconductivity of $HCaB_3$.

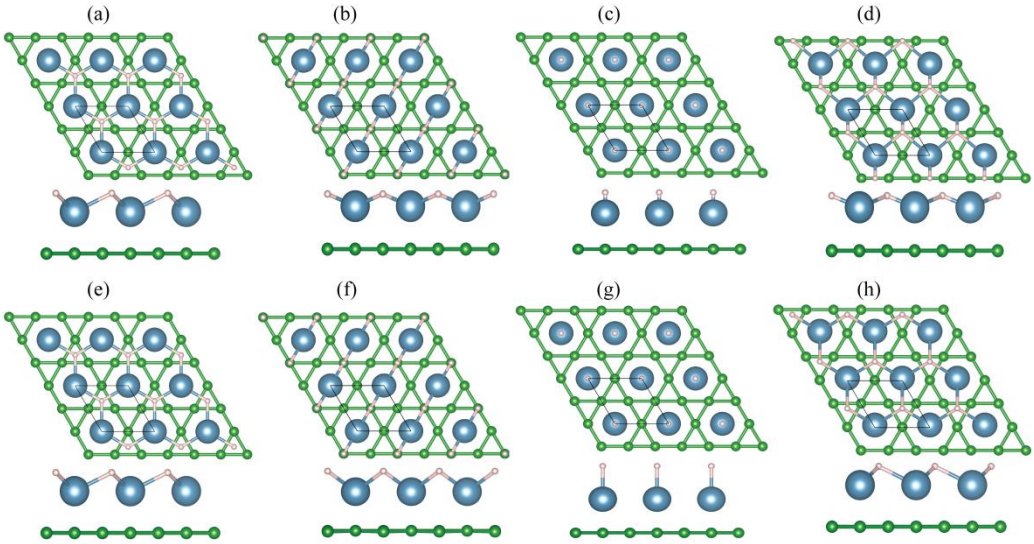

Fig. S2 (a-d) Initial positions of H atoms above the center of triangle formed by B atoms, above the B and Ca atoms, and above the B-B bonds. (e-h) Corresponding final positions of H atoms after full relaxation. Green, blue, and pink spheres represent B, Ca, and H atoms, respectively.

4. Electron localization function (ELF) of MB_3 (M = Be, Ca, Sr) and $HCaB_3$

The ELF value ranges from 0 to 1. Generally, 0 indicates very low electron density, 1 indicates strong covalent bonding or lone pair electrons, and 0.5 indicates homogeneity of electron gas. The 2D maps of ELF for MB_3 (M = Be, Ca, Sr) and $HCaB_3$ are shown in Fig. S3, in which electron distributions in (001), (010) and (110) crystal plane are shown. The ELF values are about 0.7-0.9 between neighboring B atoms for these monolayers in Figs. S3 (1), (5), (9), and (13), suggesting the strong covalent bonds between B atoms. The ELF values in the metal layers in Figs. S3(2), (6), (10), and (14) are different. That is, the homogeneous gas in the Be layer in Fig. S3(2) suggests that there are strong interactions between Be-Be atoms. However, for CaB_3, the ELF value in the Ca layer between the nearest Ca atoms is about 0.1-0.3 as shown in Figs. S3(6, 14). For SrB_3 , the ELF value in the Sr layer between the nearest Sr atoms is about 0.1-0.2 as shown in Fig. S3(10). Above results indicate very weak interactions between Ca-Ca and Sr-Sr atoms.

The ELF value between B atom and Be atom in Fig. S3(3) is 0.7-0.8, and the Bader charge value of Be is 0.456 *e*, showing that there is an obvious charge transfer from Be atom to the adjacent B atoms. Above two aspects together indicate the strong covalent bonds between B and Be atoms. As shown in Figs. S3(7), (11), the small ELF values between the B atoms and the Ca/Sr atoms and Bader charge analysis shows 0.728/0.624 *e* transfer from each Ca/Sr atom to the boron kagome layer, suggesting that Ca-B and Sr-B form ionic bonds. After hydrogen absorption on CaB_3, as shown in Figs. S3(15, 16), the ELF values in the middle of Ca-B bonds and Ca-H bonds

are about 0.1-0.2, and the Bader charge analysis shows 1.331 *e* transfer from Ca atom, including 0.628 *e* to B kagome layer and 0.703 *e* to H layer, which indicate the formation of Ca-B and Ca-H ionic bonds.

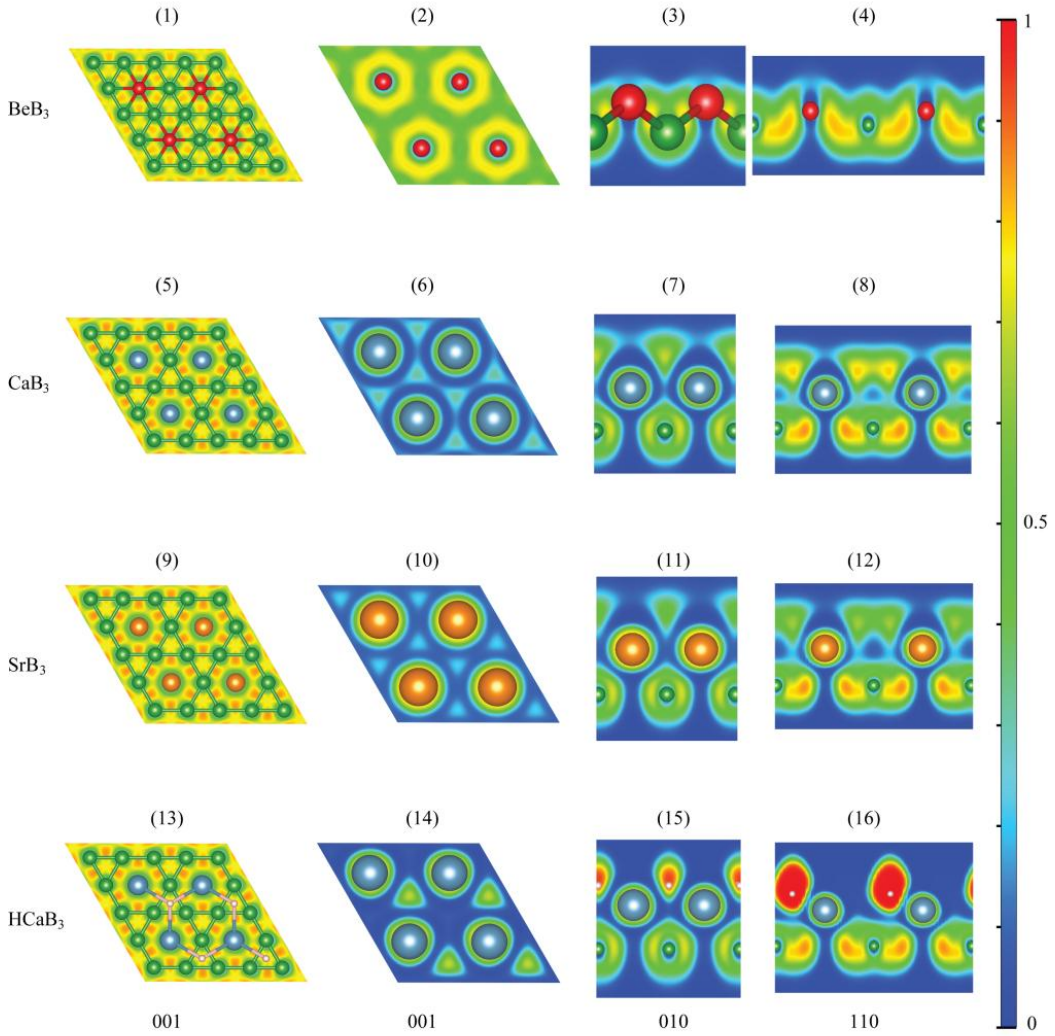

Fig. S3: 2D maps of ELF for MB_3 and $HCaB_3$. (1-4) for BeB_3, (5-8) for CaB_3, (9-12) for SrB_3 and (13-16) for $HCaB_3$. The color of red and blue refer to the highest (1.0) and lowest (0.0) value of ELF, indicating accumulation and depletion of electrons, respectively.

5. Electronic structure of BeB_3 and SrB_3

For BeB_3 and SrB_3, some bands cross the Fermi level, supporting that BeB_3 and SrB_3 are metal shown in Figs. S4(a, b) and Figs. S4(e, f). As shown in Figs. S4(c, d), the states around the Fermi level are mainly contributed by B-*p* orbitals, followed by the Be-*p* orbitals. For SrB_3, the states around the Fermi level are mainly contributed by B-*p* orbitals, followed by the Sr-*d* orbitals.

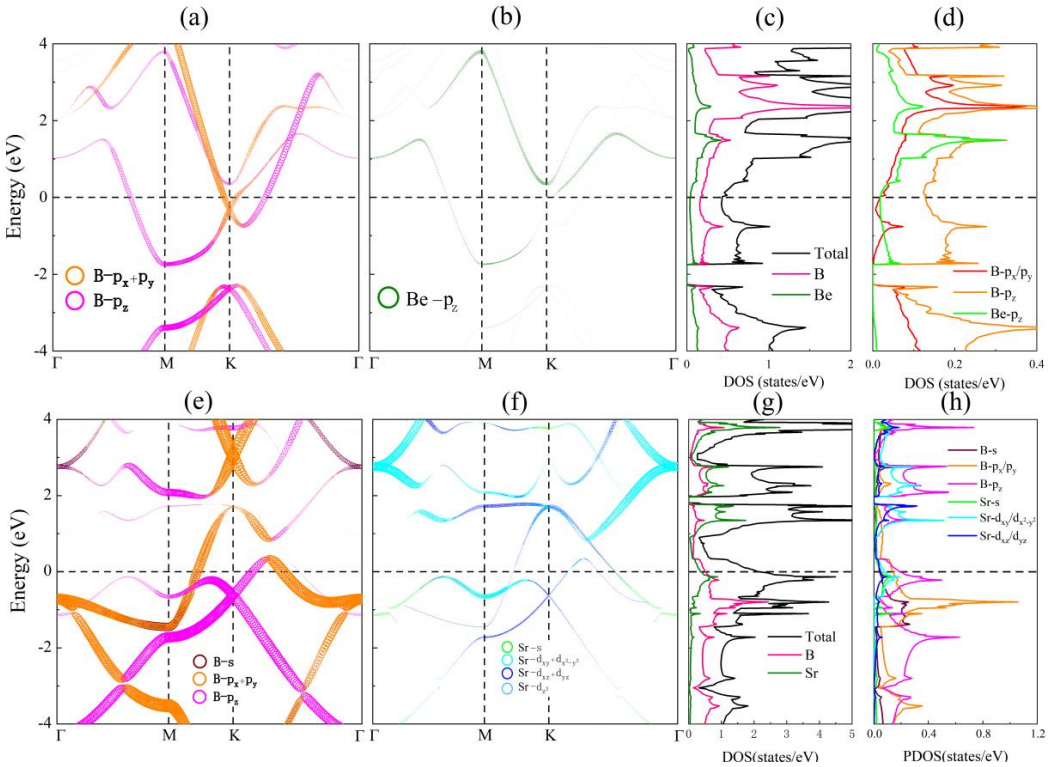

Fig. S4: Orbital-projected band structure of B (a) and Be (b) for BeB_3 along high-symmetry line Γ - M - K -Γ. The total DOS of BeB_3 and the total DOS of B and Be (c). Orbital-projected DOS of BeB_3 (d). (e) - (h) are the similar with (a) - (d) but for SrB_3.

6. Electron-phonon coupling and possible superconductivity of BeB_3 and SrB_3

In the unit cell, there are four atoms leading to twelve phonon bands, which include three acoustic phonon modes and nine optical phonon modes. The range of frequency extending up to about 1214 cm^{-1} for BeB_3 and 1048 cm^{-1} for SrB_3, respectively. Phonon dispersion weighted by the vibration modes of B, *M* (*M* = Be, Sr) atoms of BeB_3 and SrB_3 are shown in Figs. S5(a) and S5(e). For BeB_3, the region with the largest λ_{qv} is in the low-frequency shows in Fig. S5(b) and in Fig. S5(d). Eliashberg spectral function of BeB_3 indicates that its EPC mainly comes from the coupling between electrons and the low-frequency out-of-plane vibrations of B and Be atoms. For SrB_3, the region with the largest λ_{qv} is also in the low frequency shows in Fig. S5(f) and in Fig. S5(h). Eliashberg spectral function of SrB_3 indicates that its EPC also mainly comes from the coupling between electrons and the low-frequency out-of-plane vibrations of B and Sr atoms. Particularly, the in-plane vibration of B also contributes greatly, as seen from the strong EPC λ_{qv} at the soften phonon spectrum along Γ-M direction.

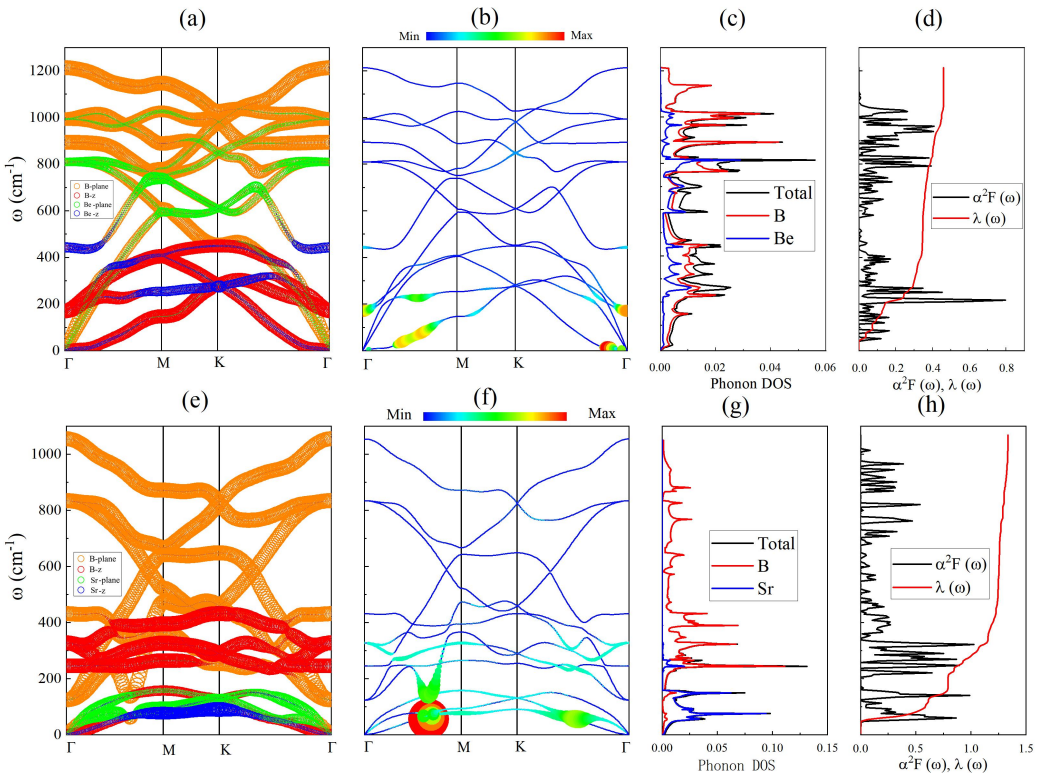

Fig. S5: Phonon dispersion weighted by the vibration modes of the atoms for BeB_3 (a) and SrB_3 (e). Phonon dispersion weighted by the magnitude of EPC λ_{qv} for BeB_3 (b) and SrB_3 (f). Atom-projected phonon DOS for BeB_3 (c) and SrB_3 (g). Eliashberg spectral function $\alpha^2F(\omega)$ and cumulative frequency dependence of EPC $\lambda(\omega)$ of BeB_3 (d) and SrB_3 (h).

7. The vibration modes of MB_3 (M = Be, Ca, Sr) and $HCaB_3$ at Γ point

The modes at Γ point for BeB_3, CaB_3, SrB_3, and $HCaB_3$ are shown in Figs. S6-S9. Figs. S6-S9 (1-3) show the acoustic phonon modes at zero frequency. The direction of each acoustic vibration modes are same with the same amplitude. The rests of vibration modes are optical phonon modes, revealing the relative vibrations of B and metal atoms. More information about the vibration modes at Γ point, including the symmetry, vibration, Raman/infrared activity and frequencies for BeB_3, CaB_3, SrB_3, $HCaB_3$ are listed in Table S1-S4, which provide a theoretical basis for future experimental verification.

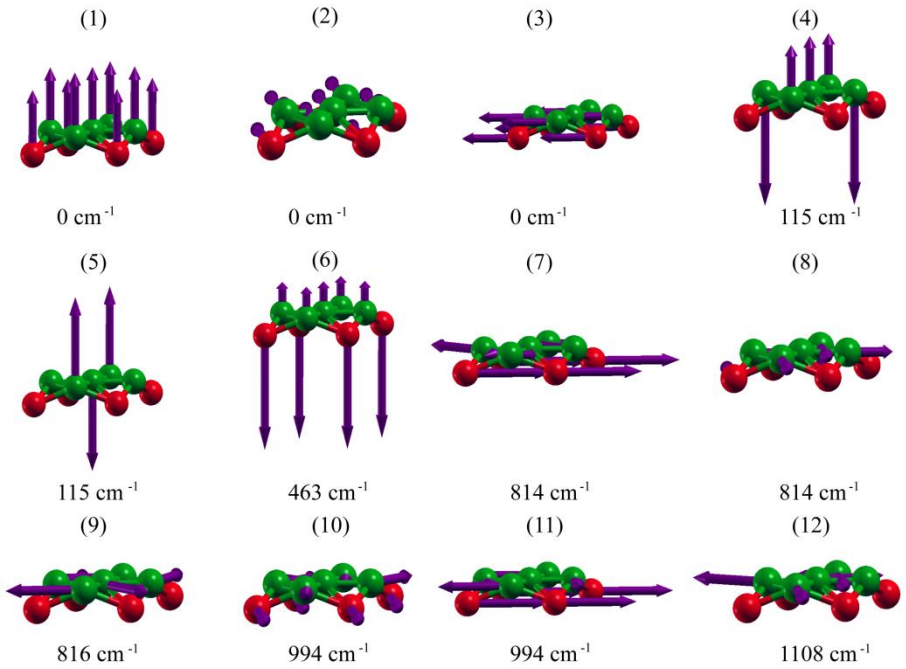

Fig. S6: The twelve vibration modes of pristine BeB_3 at Γ point are in the Brillouin zone. The vibration frequencies are shown below each figure. The rad and green spheres represent Be and B atoms, respectively, and the purple arrow represents the direction of atoms vibration.

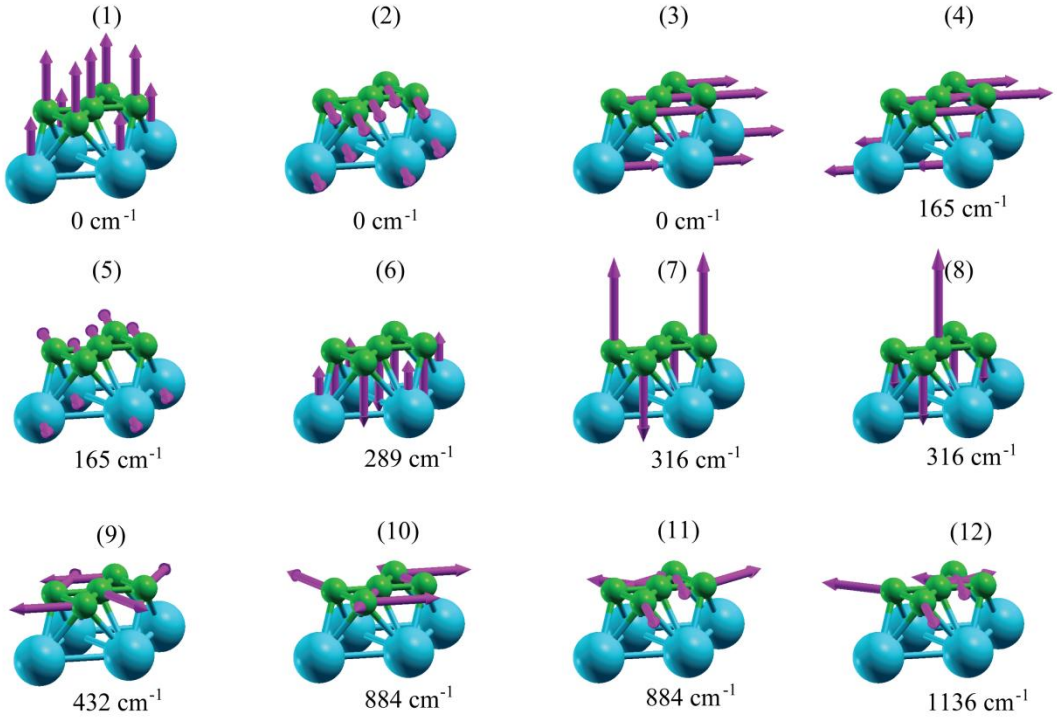

Fig. S7: The twelve vibration modes of pristine CaB_3 at Γ point are in the Brillouin zone. The vibration frequencies are shown below each figure. The blue and green spheres represent Ca and B atoms, respectively, and the purple arrow represents the direction of atoms vibration.

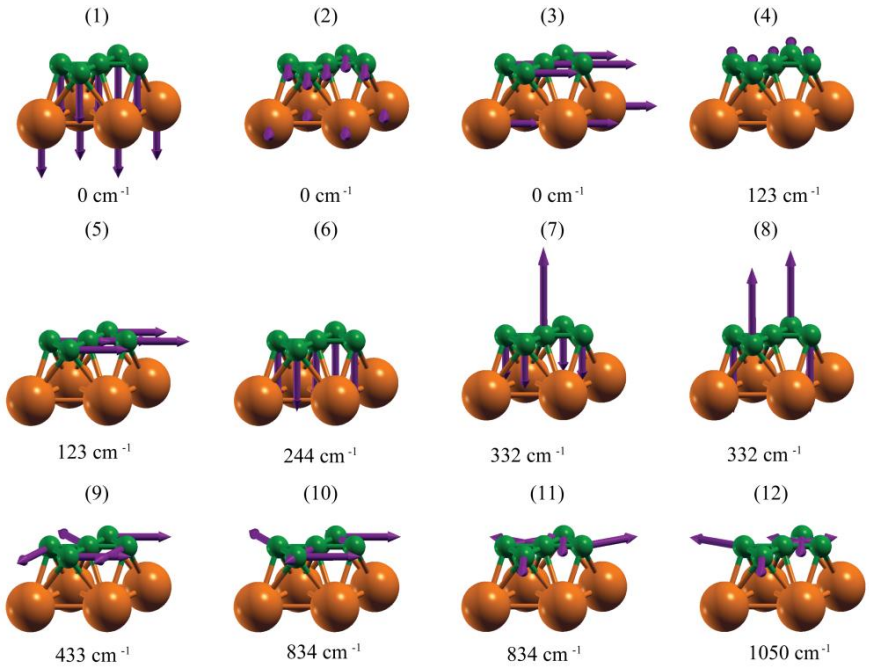

Fig. S8: The twelve vibration modes of pristine SrB_3 at Γ point are in the Brillouin zone. The vibration frequencies are shown below each figure. The orange and green spheres represent Sr and B atoms, respectively, and the purple arrow represents the direction of atoms vibration.

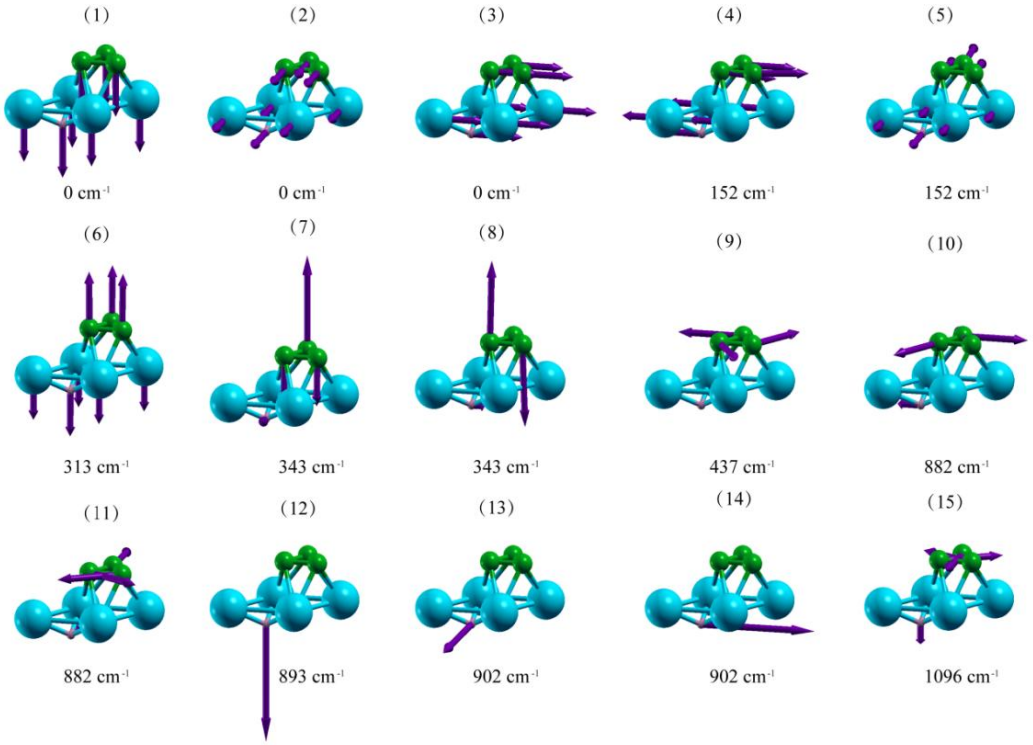

Fig. S9: The fifteen vibration modes of pristine $HCaB_3$ at Γ point are in the Brillouin zone. The vibration frequencies are shown below each figure. The blue, pink, and green spheres represent Sr, H and B atoms, respectively, and the purple arrow represents the direction of atoms vibration.

TABLE S1: The symmetry, vibration, activity (I is Infrared, and R is Raman) and frequency (cm^{-1}) for the 12 vibration modes at Γ point of BeB_3.

Modes	Symmetry	Vibration	Activity	Freq. (cm^{-1})
1	A_1	Translational	I+R	0
2-3	E_1	Translational	I+R	0
4-5	E_2	Out-plane B and Be	R	155
6	A_1	Out-plane B and Be	I+R	463
7-8	E_1	In-plane B and Be	I+R	814
9	B_2	In-plane B	-	816
10-11	E_1	In-plane B and Be	I+R	944
12	B_1	In-plane B	-	1108

TABLE S2: The symmetry, vibration, activity(I is Infrared, and R is Raman) and frequency (cm^{-1}) for the 12 vibration modes at Γ point of CaB_3.

Modes	Symmetry	Vibration	Activity	Freq. (cm^{-1})
1	A_1	Translational	I+R	0
2-3	E_1	Translational	I+R	0
4-5	E_1	In-plane B and Sr	I+R	165
6	A_1	Out-of-plane B and Ca	I+R	289
7-8	E_2	Out-of-plane B and Ca	R	316
9	B_2	In-plane B	-	432
10-11	E_1	In-plane B	I+R	884
12	B_1	In-plane B	-	1136

TABLE S3: The symmetry, vibration, activity (I is Infrared, and R is Raman) and frequency (cm^{-1}) for the 12 vibration modes at Γ point of SrB_3.

Modes	Symmetry	Vibration	Activity	Freq. (cm^{-1})
1	A_1	Translational	I+R	0
2-3	E_1	Translational	I+R	0
4-5	E_1	In-plane B and Sr	I+R	123
6	A_1	Out-of-plane B and Sr	I+R	244
7-8	E_2	Out-of-plane B and Sr	R	332
9	B_2	In-plane B	-	433
10-11	E_1	In-plane B	I+R	834
12	B_1	In-plane B	-	1050

TABLE S4: The symmetry, vibration, activity (I is Infrared, and R is Raman) and frequency (cm^{-1}) for the 15 vibration modes at Γ point of $HCaB_3$.

Modes	Symmetry	Vibration	Activity	Freq. (cm^{-1})
1	A_1	Translational	I+R	0
2-3	E	Translational	I+R	0
4-5	E	In-plane B, Ca and H	I+R	152
6	A_1	Out-of-plane B, Ca and H	I+R	313
7-8	E	Out-of-plane B and Ca, In-plane H	I+R	343
9	A_2	In-plane B	-	438
10-11	E	In-plane B and H	I+R	882
12	A_1	Out-of-plane H	I+R	893
13-14	E	In-plane H	I+R	902
15	A_1	In-plane B, Out-plane H	I+R	1096

8. T_c of BeB_3, CaB_3, SrB_3 , and $HCaB_3$ as a function of Coulomb pseudopotential μ*

The Coulomb pseudopotential μ* is a parameter closely related to T_c [8], which are shown in Eq. (5). Here, the relationship between Tc and μ* of BeB_3, CaB_3, SrB_3 , and $HCaB_3$ are studied in detail by setting μ* in the range of 0.05-0.15. As shown in Fig. S10, for BeB_3, CaB_3, SrB_3 , and $HCaB_3$, T_c monotonically decreases with the increase of μ* . For BeB_3, CaB_3 and SrB_3, when μ* increases from 0.05 to 0.15, T_c decreases from 6.7 K to 1.1 K, 27.2 to 17.7 K, 24.5 K to 17.5 K, respectively. The trend of T_c for $HCaB_3$ is the same as that of MB_3, with T_c of 45.5 K at μ* = 0.05 and T_c of 33 K at μ* = 0.15. In this paper, we choose μ* = 0.1, and the T_c of BeB_3, CaB_3, SrB_3 and $HCaB_3$ are 3.2, 22.4, 20.9 and 39.3 K, respectively.

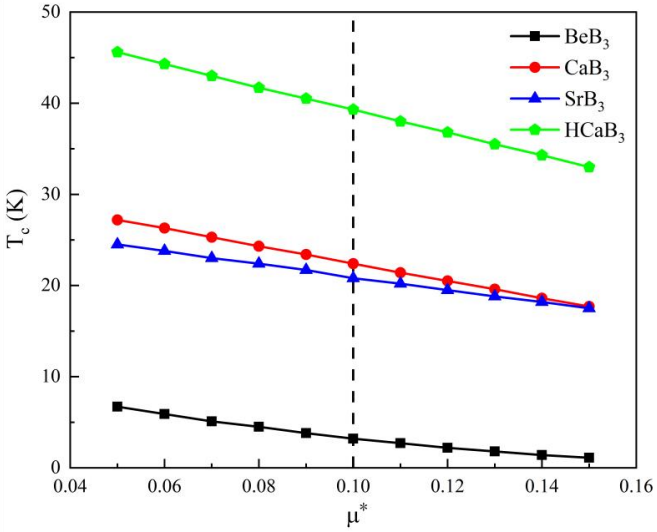

Fig. S10: Evaluated T_c of our studied two monolayers as a function of Coulomb pseudopotential μ* . Vertical line marks the value μ*=0.10 used in this work.

9. Convergence of EPC strength λ and T_c for BeB_3, CaB_3, SrB_3, and $HCaB_3$

We plot the calculated EPC strength λ and T_c as a function of the Gaussian broadening for electrons, which are shown in Figs. S11(a) and S11(b). It is seen that both λ and T_c converge for the four materials. We should determine the degauss at which λ becomes flat, and the λ at this degauss should be chosen as the convergence data[9-10]. The converged values of λ for BeB_3, CaB_3 SrB_3, and $HCaB_3$ are 0.49, 1.09, 1.33, and 1.39 at degauss of 122.4, 122.4, 204, and 68 meV, with a corresponding T_c of 3.2, 22.4, 20.9 and 39.3 K, respectively.

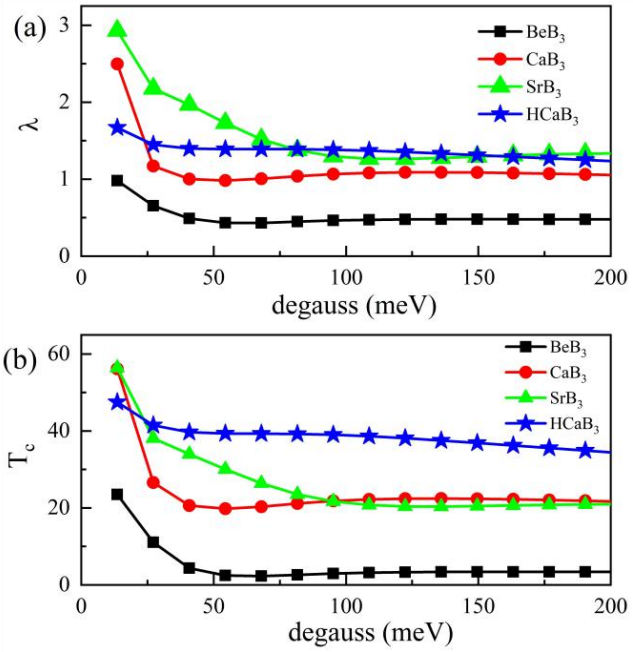

Fig. S11. λ (a) and T_c (b) as a function of degauss for pristine BeB_3, CaB_3, SrB_3, and $HCaB_3$.

10. Dynamical unstability of 2D MgB_3

We also calculate the phonon spectrum of MgB_3. Fig. S12 shows that it has an obvious imaginary frequency around M point, indicating that it is dynamically unstable.

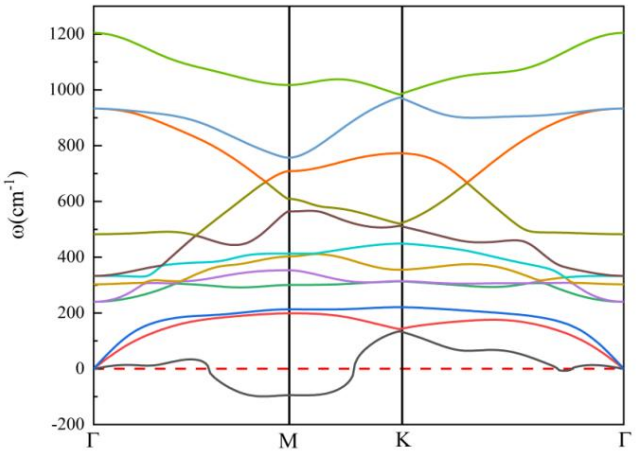

Fig. S12: Phonon dispersion of MgB_3.

Reference

[1] Kresse G, and Furthmuller J 1996 *Phys. Rev. B* **54**, 11169

[2] Paolo G, Stefano B, Nicola B, Matteo C, Roberto C, Carlo C, Davide C, Guido L C, Matteo C, Ismaila D, Andrea D C, Stefano F, Guido F, Stefano D G, Ralph G, Uwe G, Christos G, Anton K, Michele L, Martin-Samos Layla, Nicola M, Francesco M, Riccardo M, Stefano P, Alfredo P, Lorenzo P, Carlo S, Sandro S, Gabriele S, Ari P S, Alexander S, Paolo U, and Renata M W 2009 *J. Phys.: Condens. Matter* **21**, 395502

[3] Perdew J P, Burke K, and Ernzerhof M 1996 *Phys. Rev. Lett.* **77**, 3865

[4] Baroni S, Gironcoli S de, Corso A D, and Giannozzi P 2001 *Rev. Mod. Phys.* **73**, 515

[5] McMillan W L 1968 *Phys. Rev.* **167**, 331

[6] Dynes R C 1972 *Solid State Commun.* **10**, 615

[7] Allen P B, Dynes R C 1975 *Phys. Rev. B* **12**, 905

[8] Bo T, Liu P F, Yan L, and Wang B T, 2020 Phys. Rev. Mater. **4**, 114802

[9] C. Morice, R. Akashi, T. Koretsune, S. S. Saxena, and R. Arita, 2017 *Phys. Rev. B* **95**, 180505(R)

[10] S. V. Hosseini, M. Abbasnejad, and M. R. Mohammadizadeh, 2021 *Phys. Rev. B* **104**, 224101